Measurement of the branching fraction of leptonic decay
$D_s^+ \to \tau^+ \nu_\tau$ via $\tau^+ \to \pi^+ \pi^0 \bar{\nu}_\tau$

M. Ablikim,[1] M. N. Achasov,[10,b] P. Adlarson,[67] S. Ahmed,[15] M. Albrecht,[4] R. Aliberti,[28] A. Amoroso,[66a,66c] M. R. An,[32] Q. An,[63,49] X. H. Bai,[57] Y. Bai,[48] O. Bakina,[29] R. Baldini Ferroli,[23a] I. Balossino,[24a] Y. Ban,[38,i] K. Begzsuren,[26] N. Berger,[28] M. Bertani,[23a] D. Bettoni,[24a] F. Bianchi,[66a,66c] J. Bloms,[60] A. Bortone,[66a,66c] I. Boyko,[29] R. A. Briere,[5] H. Cai,[68] X. Cai,[1,49] A. Calcaterra,[23a] G. F. Cao,[1,54] N. Cao,[1,54] S. A. Cetin,[53a] J. F. Chang,[1,49] W. L. Chang,[1,54] G. Chelkov,[29,a] D. Y. Chen,[6] G. Chen,[1] H. S. Chen,[1,54] M. L. Chen,[1,49] S. J. Chen,[35] X. R. Chen,[25] Y. B. Chen,[1,49] Z. J. Chen,[20,j] W. S. Cheng,[66c] G. Cibinetto,[24a] F. Cossio,[66c] X. F. Cui,[36] H. L. Dai,[1,49] X. C. Dai,[1,54] A. Dbeyssi,[15] R. E. de Boer,[4] D. Dedovich,[29] Z. Y. Deng,[1] A. Denig,[28] I. Denysenko,[29] M. Destefanis,[66a,66c] F. De Mori,[66a,66c] Y. Ding,[33] C. Dong,[36] J. Dong,[1,49] L. Y. Dong,[1,54] M. Y. Dong,[1,49,54] X. Dong,[68] S. X. Du,[71] Y. L. Fan,[68] J. Fang,[1,49] S. S. Fang,[1,54] Y. Fang,[1] R. Farinelli,[24a] L. Fava,[66b,66c] F. Feldbauer,[4] G. Felici,[23a] C. Q. Feng,[63,49] J. H. Feng,[50] M. Fritsch,[4] C. D. Fu,[1] Y. Gao,[63,49] Y. Gao,[38,i] Y. Gao,[64] Y. G. Gao,[6] I. Garzia,[24a,24b] P. T. Ge,[68] C. Geng,[50] E. M. Gersabeck,[58] A. Gilman,[61] K. Goetzen,[11] L. Gong,[33] W. X. Gong,[1,49] W. Gradl,[28] M. Greco,[66a,66c] L. M. Gu,[35] M. H. Gu,[1,49] S. Gu,[2] Y. T. Gu,[13] C. Y. Guan,[1,54] A. Q. Guo,[22] L. B. Guo,[34] R. P. Guo,[40] Y. P. Guo,[9,g] A. Guskov,[29,a] T. T. Han,[41] W. Y. Han,[32] X. Q. Hao,[16] F. A. Harris,[56] K. L. He,[1,54] F. H. Heinsius,[4] C. H. Heinz,[28] T. Held,[4] Y. K. Heng,[1,49,54] C. Herold,[51] M. Himmelreich,[11,e] T. Holtmann,[4] G. Y. Hou,[1,54] Y. R. Hou,[54] Z. L. Hou,[1] H. M. Hu,[1,54] J. F. Hu,[47,k] T. Hu,[1,49,54] Y. Hu,[1] G. S. Huang,[63,49] L. Q. Huang,[64] X. T. Huang,[41] Y. P. Huang,[1] Z. Huang,[38,i] T. Hussain,[65] N. Hüsken,[22,28] W. Ikegami Andersson,[67] W. Imoehl,[22] M. Irshad,[63,49] S. Jaeger,[4] S. Janchiv,[26] Q. Ji,[1] Q. P. Ji,[16] X. B. Ji,[1,54] X. L. Ji,[1,49] Y. Y. Ji,[41] H. B. Jiang,[41] X. S. Jiang,[1,49,54] J. B. Jiao,[41] Z. Jiao,[18] S. Jin,[35] Y. Jin,[57] M. Q. Jing,[1,54] T. Johansson,[67] N. Kalantar-Nayestanaki,[55] X. S. Kang,[33] R. Kappert,[55] M. Kavatsyuk,[55] B. C. Ke,[43,1] I. K. Keshk,[4] A. Khoukaz,[60] P. Kiese,[28] R. Kiuchi,[1] R. Kliemt,[11] L. Koch,[30] O. B. Kolcu,[53a,d] B. Kopf,[4] M. Kuemmel,[4] M. Kuessner,[4] A. Kupsc,[67] M. G. Kurth,[1,54] W. Kühn,[30] J. J. Lane,[58] J. S. Lange,[30] P. Larin,[15] A. Lavania,[21] L. Lavezzi,[66a,66c] Z. H. Lei,[63,49] H. Leithoff,[28] M. Lellmann,[28] T. Lenz,[28] C. Li,[39] C. H. Li,[32] Cheng Li,[63,49] D. M. Li,[71] F. Li,[1,49] G. Li,[1] H. Li,[43] H. Li,[63,49] H. B. Li,[1,54] H. J. Li,[16] J. L. Li,[41] J. Q. Li,[4] J. S. Li,[50] Ke Li,[1] L. K. Li,[1] Lei Li,[3] P. R. Li,[31,l,m] S. Y. Li,[52] W. D. Li,[1,54] W. G. Li,[1] X. H. Li,[63,49] X. L. Li,[41] Xiaoyu Li,[1,54] Z. Y. Li,[50] H. Liang,[63,49] H. Liang,[1,54] H. Liang,[27] Y. F. Liang,[45] Y. T. Liang,[25] G. R. Liao,[12] L. Z. Liao,[1,54] J. Libby,[21] C. X. Lin,[50] B. J. Liu,[1] C. X. Liu,[1] D. Liu,[15,63] F. H. Liu,[44] Fang Liu,[1] Feng Liu,[6] H. B. Liu,[13] H. M. Liu,[1,54] Huanhuan Liu,[1] Huihui Liu,[17] J. B. Liu,[63,49] J. L. Liu,[64] J. Y. Liu,[1,54] K. Liu,[1] K. Y. Liu,[33] L. Liu,[63,49] M. H. Liu,[9,g] P. L. Liu,[1] Q. Liu,[68] Q. Liu,[54] S. B. Liu,[63,49] Shuai Liu,[46] T. Liu,[1,54] W. M. Liu,[63,49] X. Liu,[31,l,m] Y. Liu,[31,l,m] Y. B. Liu,[36] Z. A. Liu,[1,49,54] Z. Q. Liu,[41] X. C. Lou,[1,49,54] F. X. Lu,[50] H. J. Lu,[18] J. D. Lu,[1,54] J. G. Lu,[1,49] X. L. Lu,[1] Y. Lu,[1] Y. P. Lu,[1,49] C. L. Luo,[34] M. X. Luo,[70] P. W. Luo,[50] T. Luo,[9,g] X. L. Luo,[1,49] X. R. Lyu,[54] F. C. Ma,[33] H. L. Ma,[1] L. L. Ma,[41] M. M. Ma,[1,54] Q. M. Ma,[1] R. Q. Ma,[1] R. T. Ma,[54] X. X. Ma,[1,54] X. Y. Ma,[1,49] F. E. Maas,[15] M. Maggiora,[66a,66c] S. Maldaner,[4] S. Malde,[61] Q. A. Malik,[65] A. Mangoni,[23b] Y. J. Mao,[38,i] Z. P. Mao,[1] S. Marcello,[66a,66c] Z. X. Meng,[57] J. G. Messchendorp,[55] G. Mezzadri,[24a] T. J. Min,[35] R. E. Mitchell,[22] X. H. Mo,[1,49,54] Y. J. Mo,[6] N. Yu. Muchnoi,[10,b] H. Muramatsu,[59] S. Nakhoul,[11,e] Y. Nefedov,[29] F. Nerling,[11,e] I. B. Nikolaev,[10,b] Z. Ning,[1,49] S. Nisar,[8,h] S. L. Olsen,[54] Q. Ouyang,[1,49,54] S. Pacetti,[23b,23c] X. Pan,[9,g] Y. Pan,[58] A. Pathak,[1] A. Pathak,[27] P. Patteri,[23a] M. Pelizaeus,[4] H. P. Peng,[63,49] K. Peters,[11,e] J. Pettersson,[67] J. L. Ping,[34] R. G. Ping,[1,54] R. Poling,[59] V. Prasad,[63,49] H. Qi,[63,49] H. R. Qi,[52] K. H. Qi,[25] M. Qi,[35] T. Y. Qi,[9] S. Qian,[1,49] W. B. Qian,[54] Z. Qian,[50] C. F. Qiao,[54] L. Q. Qin,[12] X. P. Qin,[9] X. S. Qin,[41] Z. H. Qin,[1,49] J. F. Qiu,[1] S. Q. Qu,[36] K. H. Rashid,[65] K. Ravindran,[21] C. F. Redmer,[28] A. Rivetti,[66c] V. Rodin,[55] M. Rolo,[66c] G. Rong,[1,54] Ch. Rosner,[15] M. Rump,[60] H. S. Sang,[63] A. Sarantsev,[29,c] Y. Schelhaas,[28] C. Schnier,[4] K. Schoenning,[67] M. Scodeggio,[24a,24b] D. C. Shan,[46] W. Shan,[19] X. Y. Shan,[63,49] J. F. Shangguan,[46] M. Shao,[63,49] C. P. Shen,[9] H. F. Shen,[1,54] P. X. Shen,[36] X. Y. Shen,[1,54] H. C. Shi,[63,49] R. S. Shi,[1,54] X. Shi,[1,49] X. D. Shi,[63,49] J. J. Song,[41] W. M. Song,[27,1] Y. X. Song,[38,i] S. Sosio,[66a,66c] S. Spataro,[66a,66c] K. X. Su,[68] P. P. Su,[46] F. F. Sui,[41] G. X. Sun,[1] H. K. Sun,[1] J. F. Sun,[16] L. Sun,[68] S. S. Sun,[1,54] T. Sun,[1,54] W. Y. Sun,[27] W. Y. Sun,[34] X. Sun,[20,j] Y. J. Sun,[63,49] Y. K. Sun,[63,49] Y. Z. Sun,[1] Z. T. Sun,[1] Y. H. Tan,[68] Y. X. Tan,[63,49] C. J. Tang,[45] G. Y. Tang,[1] J. Tang,[50] J. X. Teng,[63,49] V. Thoren,[67] W. H. Tian,[43] Y. T. Tian,[25] I. Uman,[53b] B. Wang,[1] C. W. Wang,[35] D. Y. Wang,[38,i] H. J. Wang,[31,l,m] H. P. Wang,[1,54] K. Wang,[1,49] L. L. Wang,[1] M. Wang,[41] M. Z. Wang,[38,i] Meng Wang,[1,54] W. Wang,[50] W. H. Wang,[68] W. P. Wang,[63,49] X. Wang,[38,i] X. F. Wang,[31,l,m] X. L. Wang,[9,g] Y. Wang,[63,49] Y. Wang,[50] Y. D. Wang,[37] Y. F. Wang,[1,49,54] Y. Q. Wang,[1] Y. Y. Wang,[31,l,m] Z. Wang,[1,49] Z. Y. Wang,[1] Ziyi Wang,[54] Zongyuan Wang,[1,54] D. H. Wei,[12] F. Weidner,[60] S. P. Wen,[1] D. J. White,[58] U. Wiedner,[4] G. Wilkinson,[61] M. Wolke,[67] L. Wollenberg,[4] J. F. Wu,[1,54] L. H. Wu,[1] L. J. Wu,[1,54] X. Wu,[9,g] Z. Wu,[1,49] L. Xia,[63,49] H. Xiao,[9,g] S. Y. Xiao,[1] Z. J. Xiao,[34] X. H. Xie,[38,i] Y. G. Xie,[1,49] Y. H. Xie,[6] T. Y. Xing,[1,54] G. F. Xu,[1] Q. J. Xu,[14] W. Xu,[1,54] X. P. Xu,[46] Y. C. Xu,[54] F. Yan,[9,g] L. Yan,[9,g] W. B. Yan,[63,49] W. C. Yan,[71] Xu Yan,[46] H. J. Yang,[42,f] H. X. Yang,[1] L. Yang,[43] S. L. Yang,[54] Y. X. Yang,[12] Yifan Yang,[1,54] Zhi Yang,[25] M. Ye,[1,49] M. H. Ye,[7] J. H. Yin,[1] Z. Y. You,[50] B. X. Yu,[1,49,54] C. X. Yu,[36] G. Yu,[1,54] J. S. Yu,[20,j] T. Yu,[64] C. Z. Yuan,[1,54] L. Yuan,[2] X. Q. Yuan,[38,i] Y. Yuan,[1] Z. Y. Yuan,[50]

C. X. Yue,[32] A. A. Zafar,[65] X. Zeng Zeng,[6] Y. Zeng,[20,j] A. Q. Zhang,[1] B. X. Zhang,[1] Guangyi Zhang,[16] H. Zhang,[63] H. H. Zhang,[50] H. H. Zhang,[27] H. Y. Zhang,[1,49] J. J. Zhang,[43] J. L. Zhang,[69] J. Q. Zhang,[34] J. W. Zhang,[1,49,54] J. Y. Zhang,[1] J. Z. Zhang,[1,54] Jianyu Zhang,[1,54] Jiawei Zhang,[1,54] L. M. Zhang,[52] L. Q. Zhang,[50] Lei Zhang,[35] S. Zhang,[50] S. F. Zhang,[35] Shulei Zhang,[20,j] X. D. Zhang,[37] X. Y. Zhang,[41] Y. Zhang,[61] Y. T. Zhang,[71] Y. H. Zhang,[1,49] Yan Zhang,[63,49] Yao Zhang,[1] Z. H. Zhang,[6] Z. Y. Zhang,[68] G. Zhao,[1] J. Zhao,[32] J. Y. Zhao,[1,54] J. Z. Zhao,[1,49] Lei Zhao,[63,49] Ling Zhao,[1] M. G. Zhao,[36] Q. Zhao,[1] S. J. Zhao,[71] Y. B. Zhao,[1,49] Y. X. Zhao,[25] Z. G. Zhao,[63,49] A. Zhemchugov,[29,a] B. Zheng,[64] J. P. Zheng,[1,49] Y. Zheng,[38,i] Y. H. Zheng,[54] B. Zhong,[34] C. Zhong,[64] L. P. Zhou,[1,54] Q. Zhou,[1,54] X. Zhou,[68] X. K. Zhou,[54] X. R. Zhou,[63,49] X. Y. Zhou,[32] A. N. Zhu,[1,54] J. Zhu,[36] K. Zhu,[1] K. J. Zhu,[1,49,54] S. H. Zhu,[62] T. J. Zhu,[69] W. J. Zhu,[36] W. J. Zhu,[9,g] Y. C. Zhu,[63,49] Z. A. Zhu,[1,54] B. S. Zou,[1] and J. H. Zou[1]

(BESIII Collaboration)

[1]*Institute of High Energy Physics, Beijing 100049, People's Republic of China*
[2]*Beihang University, Beijing 100191, People's Republic of China*
[3]*Beijing Institute of Petrochemical Technology, Beijing 102617, People's Republic of China*
[4]*Bochum Ruhr-University, D-44780 Bochum, Germany*
[5]*Carnegie Mellon University, Pittsburgh, Pennsylvania 15213, USA*
[6]*Central China Normal University, Wuhan 430079, People's Republic of China*
[7]*China Center of Advanced Science and Technology, Beijing 100190, People's Republic of China*
[8]*COMSATS University Islamabad, Lahore Campus, Defence Road, Off Raiwind Road,*
54000 Lahore, Pakistan
[9]*Fudan University, Shanghai 200443, People's Republic of China*
[10]*G.I. Budker Institute of Nuclear Physics SB RAS (BINP), Novosibirsk 630090, Russia*
[11]*GSI Helmholtzcentre for Heavy Ion Research GmbH, D-64291 Darmstadt, Germany*
[12]*Guangxi Normal University, Guilin 541004, People's Republic of China*
[13]*Guangxi University, Nanning 530004, People's Republic of China*
[14]*Hangzhou Normal University, Hangzhou 310036, People's Republic of China*
[15]*Helmholtz Institute Mainz, Staudinger Weg 18, D-55099 Mainz, Germany*
[16]*Henan Normal University, Xinxiang 453007, People's Republic of China*
[17]*Henan University of Science and Technology, Luoyang 471003, People's Republic of China*
[18]*Huangshan College, Huangshan 245000, People's Republic of China*
[19]*Hunan Normal University, Changsha 410081, People's Republic of China*
[20]*Hunan University, Changsha 410082, People's Republic of China*
[21]*Indian Institute of Technology Madras, Chennai 600036, India*
[22]*Indiana University, Bloomington, Indiana 47405, USA*
[23a]*INFN Laboratori Nazionali di Frascati, I-00044, Frascati, Italy*
[23b]*INFN Laboratori Nazionali di Frascati, INFN Sezione di Perugia, I-06100, Perugia, Italy*
[23c]*INFN Laboratori Nazionali di Frascati, University of Perugia, I-06100, Perugia, Italy*
[24a]*INFN Sezione di Ferrara, INFN Sezione di Ferrara, I-44122, Ferrara, Italy*
[24b]*INFN Sezione di Ferrara, University of Ferrara, I-44122, Ferrara, Italy*
[25]*Institute of Modern Physics, Lanzhou 730000, People's Republic of China*
[26]*Institute of Physics and Technology, Peace Ave. 54B, Ulaanbaatar 13330, Mongolia*
[27]*Jilin University, Changchun 130012, People's Republic of China*
[28]*Johannes Gutenberg University of Mainz, Johann-Joachim-Becher-Weg 45, D-55099 Mainz, Germany*
[29]*Joint Institute for Nuclear Research, 141980 Dubna, Moscow region, Russia*
[30]*Justus-Liebig-Universitaet Giessen, II. Physikalisches Institut, Heinrich-Buff-Ring 16,*
D-35392 Giessen, Germany
[31]*Lanzhou University, Lanzhou 730000, People's Republic of China*
[32]*Liaoning Normal University, Dalian 116029, People's Republic of China*
[33]*Liaoning University, Shenyang 110036, People's Republic of China*
[34]*Nanjing Normal University, Nanjing 210023, People's Republic of China*
[35]*Nanjing University, Nanjing 210093, People's Republic of China*
[36]*Nankai University, Tianjin 300071, People's Republic of China*
[37]*North China Electric Power University, Beijing 102206, People's Republic of China*
[38]*Peking University, Beijing 100871, People's Republic of China*
[39]*Qufu Normal University, Qufu 273165, People's Republic of China*
[40]*Shandong Normal University, Jinan 250014, People's Republic of China*
[41]*Shandong University, Jinan 250100, People's Republic of China*
[42]*Shanghai Jiao Tong University, Shanghai 200240, People's Republic of China*

[43]*Shanxi Normal University, Linfen 041004, People's Republic of China*
[44]*Shanxi University, Taiyuan 030006, People's Republic of China*
[45]*Sichuan University, Chengdu 610064, People's Republic of China*
[46]*Soochow University, Suzhou 215006, People's Republic of China*
[47]*South China Normal University, Guangzhou 510006, People's Republic of China*
[48]*Southeast University, Nanjing 211100, People's Republic of China*
[49]*State Key Laboratory of Particle Detection and Electronics, Beijing 100049, Hefei 230026,*
People's Republic of China
[50]*Sun Yat-Sen University, Guangzhou 510275, People's Republic of China*
[51]*Suranaree University of Technology, University Avenue 111, Nakhon Ratchasima 30000, Thailand*
[52]*Tsinghua University, Beijing 100084, People's Republic of China*
[53a]*Turkish Accelerator Center Particle Factory Group, Istanbul Bilgi University, HEP Res. Cent.,*
34060 Eyup, Istanbul, Turkey
[53b]*Turkish Accelerator Center Particle Factory Group, Near East University,*
Nicosia, North Cyprus, Mersin 10, Turkey
[54]*University of Chinese Academy of Sciences, Beijing 100049, People's Republic of China*
[55]*University of Groningen, NL-9747 AA Groningen, The Netherlands*
[56]*University of Hawaii, Honolulu, Hawaii 96822, USA*
[57]*University of Jinan, Jinan 250022, People's Republic of China*
[58]*University of Manchester, Oxford Road, Manchester, M13 9PL, United Kingdom*
[59]*University of Minnesota, Minneapolis, Minnesota 55455, USA*
[60]*University of Muenster, Wilhelm-Klemm-Str. 9, 48149 Muenster, Germany*
[61]*University of Oxford, Keble Rd, Oxford, United Kingdom OX13RH*
[62]*University of Science and Technology Liaoning, Anshan 114051, People's Republic of China*
[63]*University of Science and Technology of China, Hefei 230026, People's Republic of China*
[64]*University of South China, Hengyang 421001, People's Republic of China*
[65]*University of the Punjab, Lahore-54590, Pakistan*
[66a]*University of Turin and INFN, University of Turin, I-10125, Turin, Italy*
[66b]*University of Turin and INFN, University of Eastern Piedmont, I-15121, Alessandria, Italy*
[66c]*University of Turin and INFN, INFN, I-10125, Turin, Italy*
[67]*Uppsala University, Box 516, SE-75120 Uppsala, Sweden*
[68]*Wuhan University, Wuhan 430072, People's Republic of China*
[69]*Xinyang Normal University, Xinyang 464000, People's Republic of China*
[70]*Zhejiang University, Hangzhou 310027, People's Republic of China*
[71]*Zhengzhou University, Zhengzhou 450001, People's Republic of China*

By analyzing 6.32 fb^{-1} of e^+e^- annihilation data collected at the center-of-mass energies between 4.178 and 4.226 GeV with the BESIII detector, we determine the branching fraction of the leptonic decay $D_s^+ \to \tau^+ \nu_\tau$, with $\tau^+ \to \pi^+ \pi^0 \bar{\nu}_\tau$, to be $\mathcal{B}_{D_s^+ \to \tau^+ \nu_\tau} = (5.29 \pm 0.25_{\text{stat}} \pm 0.20_{\text{syst}})\%$. We estimate the product

[a]Also at the Moscow Institute of Physics and Technology, Moscow 141700, Russia.
[b]Also at the Novosibirsk State University, Novosibirsk, 630090, Russia.
[c]Also at the NRC "Kurchatov Institute", PNPI, 188300, Gatchina, Russia.
[d]Currently at Istanbul Arel University, 34295 Istanbul, Turkey.
[e]Also at Goethe University Frankfurt, 60323 Frankfurt am Main, Germany.
[f]Also at Key Laboratory for Particle Physics, Astrophysics and Cosmology, Ministry of Education; Shanghai Key Laboratory for Particle Physics and Cosmology; Institute of Nuclear and Particle Physics, Shanghai 200240, People's Republic of China.
[g]Also at Key Laboratory of Nuclear Physics and Ion-beam Application (MOE) and Institute of Modern Physics, Fudan University, Shanghai 200443, People's Republic of China.
[h]Also at Harvard University, Department of Physics, Cambridge, Massachusetts, 02138, USA.
[i]Also at State Key Laboratory of Nuclear Physics and Technology, Peking University, Beijing 100871, People's Republic of China.
[j]Also at School of Physics and Electronics, Hunan University, Changsha 410082, China.
[k]Also at Guangdong Provincial Key Laboratory of Nuclear Science, Institute of Quantum Matter, South China Normal University, Guangzhou 510006, China.
[l]Also at Frontiers Science Center for Rare Isotopes, Lanzhou University, Lanzhou 730000, People's Republic of China.
[m]Also at Lanzhou Center for Theoretical Physics, Lanzhou University, Lanzhou 730000, People's Republic of China.

of the Cabibbo-Kobayashi-Maskawa matrix element $|V_{cs}|$ and the D_s^+ decay constant $f_{D_s^+}$ to be $f_{D_s^+}|V_{cs}| = (244.8 \pm 5.8_{\text{stat}} \pm 4.8_{\text{syst}})$ MeV, using the known values of the τ^+ and D_s^+ masses as well as the D_s^+ lifetime, together with our branching fraction measurement. Combining the value of $|V_{cs}|$ obtained from a global fit in the standard model and $f_{D_s^+}$ from lattice quantum chromodynamics, we obtain $f_{D_s^+} = (251.6 \pm 5.9_{\text{stat}} \pm 4.9_{\text{syst}})$ MeV and $|V_{cs}| = 0.980 \pm 0.023_{\text{stat}} \pm 0.019_{\text{syst}}$. Using the branching fraction of $\mathcal{B}_{D_s^+ \to \mu^+ \nu_\mu} = (5.35 \pm 0.21) \times 10^{-3}$, we obtain the ratio of the branching fractions $\mathcal{B}_{D_s^+ \to \tau^+ \nu_\tau}/\mathcal{B}_{D_s^+ \to \mu^+ \nu_\mu} = 9.89 \pm 0.71$, which is consistent with the standard model prediction of lepton flavor universality.

I. INTRODUCTION

In the standard model, the partial width for the leptonic decay $D_s^+ \to \ell^+ \nu_\ell$ ($\ell = e$, μ or τ) is written as [1]

$$\Gamma_{D_s^+ \to \ell^+ \nu_\ell} = \frac{G_F^2}{8\pi}|V_{cs}|^2 f_{D_s^+}^2 m_\ell^2 m_{D_s^+}\left(1 - \frac{m_\ell^2}{m_{D_s^+}^2}\right)^2, \quad (1)$$

where $f_{D_s^+}$ is the D_s^+ decay constant, $|V_{cs}|$ is the Cabibbo-Kobayashi-Maskawa (CKM) matrix element describing the relative strength of c quark to s quark transition, G_F is the Fermi coupling constant, m_ℓ is the lepton mass, and $m_{D_s^+}$ is the D_s^+ mass. Charge conjugations are always included throughout this paper. The $D_s^+ \to \ell^+ \nu_\ell$ decays offer an ideal opportunity to determine $f_{D_s^+}$ or $|V_{cs}|$ in case the other has been given. Previously, the CLEO [2–4], *BABAR* [5], Belle [6], and BESIII [7–9] Collaborations have reported the measurements of the $D_s^+ \to \ell^+ \nu_\ell$ decays, giving an averaged precision for $f_{D_s^+}$ of 1.5%. In contrast, $f_{D_s^+}$ has been well calculated by lattice quantum chromodynamics (LQCD) with an uncertainty of 0.2% [10]. Improved measurements of $f_{D_s^+}$ in experiment are important to test various theoretical calculations [10–18]. Meanwhile, precise measurements of $|V_{cs}|$ are also important to test the CKM matrix unitarity [19].

On the other hand, the ratio of the branching fractions of $D_s^+ \to \tau^+ \nu_\tau$ and $D_s^+ \to \mu^+ \nu_\mu$,

$$\mathcal{R}_{\tau/\mu} = \frac{\mathcal{B}_{D_s^+ \to \tau^+ \nu_\tau}}{\mathcal{B}_{D_s^+ \to \mu^+ \nu_\mu}} = \frac{m_{\tau^+}^2\left(1 - \frac{m_{\tau^+}^2}{m_{D_s^+}^2}\right)^2}{m_{\mu^+}^2\left(1 - \frac{m_{\mu^+}^2}{m_{D_s^+}^2}\right)^2}, \quad (2)$$

in the standard model with the implication of lepton flavor universality is predicted to be 9.75 ± 0.01 using the world averages of m_τ, m_μ, and m_{D_s} [20]. In the *BABAR*, LHCb, and Belle experiments, however, hints of lepton flavor universality violation in semileptonic B decays have been reported in recent years [21–27]. Examination of lepton flavor universality in the $D_s^+ \to \ell^+ \nu_\ell$ decays is therefore important to test lepton flavor universality.

This paper reports a measurement of the branching fraction for $D_s^+ \to \tau^+ \nu_\tau$ via $\tau^+ \to \pi^+ \pi^0 \bar{\nu}_\tau$. This analysis is performed by using the data samples collected at the center-of-mass energies $\sqrt{s} = 4.178$, 4.189, 4.199, 4.209, 4.219, and 4.226 GeV with the BESIII detector. The total integrated luminosity of these data samples is 6.32 fb^{-1}.

II. BESIII DETECTOR AND MONTE CARLO SIMULATIONS

The BESIII detector [28] records symmetric e^+e^- collisions provided by the BEPCII storage ring [29], which operates with a peak luminosity of 1×10^{33} cm^{-2} s^{-1} in the center-of-mass energy range from 2.0 to 4.95 GeV. BESIII has collected large data samples in this energy region [30]. The cylindrical core of the BESIII detector covers 93% of the full solid angle and consists of a helium-based multi-layer drift chamber (MDC), a plastic scintillator time-of-flight system (TOF), and a CsI(Tl) electromagnetic calorimeter (EMC), which are all enclosed in a superconducting solenoidal magnet providing a 1.0 T magnetic field. The solenoid is supported by an octagonal flux-return yoke with resistive plate countermuon identification modules interleaved with steel. The charged-particle momentum resolution at 1 GeV/c is 0.5%, and the dE/dx resolution is 6% for electrons from Bhabha scattering. The EMC measures photon energies with a resolution of 2.5% (5%) at 1 GeV in the barrel (end cap) region. The time resolution in the TOF barrel region is 68 ps. The end cap TOF system was upgraded in 2015 using multigap resistive plate chamber technology, providing a time resolution of 60 ps [31].

Simulated data samples produced with a GEANT4-based [32] Monte Carlo (MC) package, which includes the geometric description of the BESIII detector and the detector response, are used to determine detection efficiencies and to estimate backgrounds. The simulation models the beam energy spread and initial state radiation (ISR) in the e^+e^- annihilations with the generator KKMC [33]. In the simulation, the production of open-charm processes directly produced via e^+e^- annihilations are modeled with the generator CONEXC [34], and their subsequent decays are modeled by EVTGEN [35], with known branching

fractions from the Particle Data Group [36]. The ISR production of vector charmonium(like) states and the continuum processes are incorporated in KKMC [33]. The remaining unknown charmonium decays are modeled with LUNDCHARM [37]. Final state radiation from charged final-state particles is incorporated using the PHOTOS package [38].

III. ANALYSIS METHOD

A similar double-tag (DT) method used in Refs. [9,39] is employed in this article. At $\sqrt{s}$ between 4.178 and 4.226 GeV, D_s^+ mesons are produced mainly from the processes $e^+e^- \to D_s^{*\pm}[\to \gamma(\pi^0)D_s^\pm]D_s^\mp$. We first fully reconstruct one D_s^- meson in one of several hadronic decay modes, called a single-tag candidate. We then examine the signal decay of the D_s^+ meson and the $\gamma(\pi^0)$ from D_s^{*+}, named as a double-tag candidate. At the j-th energy point, $j = 1, 2, 3, 4,$ and 5 for the energy points 4.178, 4.189, 4.199, 4.209, 4.219, and 4.226 GeV, respectively, the branching fraction for $D_s^+ \to \tau^+\nu_\tau$ is determined by

$$\mathcal{B}_{D_s^+ \to \tau^+\nu_\tau} = \frac{N_{\text{DT}}^j}{N_{\text{ST}}^j \cdot \epsilon_{\gamma(\pi^0)\tau^+\nu_\tau}^j \cdot \mathcal{B}_{\text{sub}}}. \tag{3}$$

Here, N_{DT}^j is the double-tag yield in data; $N_{\text{ST}}^j = \Sigma_i N_{\text{ST}}^{ij}$ is the total single-tag yield in data summing over tag mode i; and $\epsilon_{\gamma(\pi^0)\tau^+\nu_\tau}^j$ is the efficiency of detecting $D_s^+ \to \tau^+\nu_\tau$ in the presence of the single-tag D_s^- candidate, averaged by the single-tag yields in data. It is calculated by $\Sigma_i(N_{\text{ST}}^{ij}/N_{\text{ST}}^j) \cdot (\epsilon_{\text{DT}}^{ij}/\epsilon_{\text{ST}}^{ij})$, where $\epsilon_{\text{DT}}^{ij}$ and $\epsilon_{\text{ST}}^{ij}$ are the detection efficiencies of the double-tag and single-tag candidates, respectively. The efficiencies do not include the branching fractions for the subresonant decays. $\mathcal{B}_{\text{sub}}$ is the product of the branching fractions for the $\tau^+ \to \pi^+\pi^0\bar{\nu}_\tau$ and $\pi^0 \to \gamma\gamma$ decays.

IV. SINGLE-TAG D_s^- CANDIDATES

The single-tag D_s^- candidates are reconstructed from 14 hadronic decay modes of $D_s^- \to K^+K^-\pi^-$, $K^+K^-\pi^-\pi^0$, $K_S^0 K^-$, $K_S^0 K^-\pi^0$, $K_S^0 K_S^0\pi^-$, $K_S^0 K^+\pi^-\pi^-$, $K_S^0 K^-\pi^+\pi^-$, $\pi^+\pi^-\pi^-$, $\eta_{\gamma\gamma}\pi^-$, $\eta_{\pi^0\pi^+\pi^-}\pi^-$, $\eta'_{\eta_{\gamma\gamma}\pi^+\pi^-}\pi^-$, $\eta'_{\gamma\rho^0}\pi^-$, $\eta_{\gamma\gamma}\rho^-$, and $\eta_{\pi^+\pi^-\pi^0}\rho^-$, where the subscripts of η and η' represent the decay modes used to reconstruct η and η', respectively. Throughout this paper, ρ denotes $\rho(770)$.

The selection criteria of $K^\pm$, $\pi^\pm$, K_S^0, γ, π^0, and η are the same as those used in our previous works [8,40,41]. All charged tracks must satisfy $|V_{xy}| < 1$ cm, $|V_z| < 10$ cm, and $|\cos\theta| < 0.93$, where $|V_{xy}|$ and $|V_z|$ are a distance of the closest approach in the transverse plane and along the MDC axis, respectively, and θ is the polar angle with respect to the MDC axis. This requirement is not applied

for those from K_S^0 decays. Particle identification (PID) of the charged particles is performed with the combined dE/dx and TOF information. The confidence levels for pion and kaon hypotheses (CL_π and CL_K) are obtained. Kaon and pion candidates are required to satisfy $CL_K > CL_\pi$ and $CL_\pi > CL_K$, respectively.

The K_S^0 mesons are reconstructed via the $K_S^0 \to \pi^+\pi^-$ decays. The distances of the closest approach of the two charged pions to the interaction point are required to be less than 20 cm along the MDC axis. They are assumed to be $\pi^+\pi^-$ without PID requirements. The invariant mass of the $\pi^+\pi^-$ combination is required to be within ± 12 MeV/c^2 around the K_S^0 nominal mass [20]. The decay length of the reconstructed K_S^0 is required to be greater than twice of the vertex resolution away from the interaction point.

The π^0 and η mesons are reconstructed from photon pairs. Photon candidates are selected from the shower clusters in the EMC that are not associated with a charged track. Each electromagnetic shower is required to start within 700 ns of the event start time. The shower energy is required to be greater than 25 (50) MeV in the barrel (end cap) region of the EMC [28]. The opening angle between the candidate shower and the nearest charged track is required to be greater than 10°. To form π^0 and η candidates, the invariant masses of the selected photon pairs are required to be within the $M_{\gamma\gamma}$ interval $(0.115, 0.150)$ and $(0.50, 0.57)$ GeV/c^2, respectively. To improve momentum resolution and suppress background, a kinematic fit is imposed on each chosen photon pair to constrain its invariant mass to the π^0 or η nominal mass [20].

For the tag modes, $D_s^- \to \eta\pi^-$ and $\eta\rho^-$, the $\pi^0\pi^+\pi^-$ combinations used to form η candidates are required to be within the $M_{\pi^0\pi^+\pi^-}$ interval $(0.53, 0.57)$ GeV/c^2. To form η' candidates, we use two decay modes $\eta\pi^+\pi^-$ and $\gamma\rho^0$, whose invariant masses are required to be within the interval $(0.946, 0.970)$ GeV/c^2 and $(0.940, 0.976)$ GeV/c^2, respectively. In addition, the minimum energy of the γ from $\eta' \to \gamma\rho^0$ decays must be greater than 0.1 GeV. The ρ^0 and ρ^+ candidates are reconstructed from the $\pi^+\pi^-$ and $\pi^+\pi^0$ combinations with invariant masses within the interval $(0.57, 0.97)$ GeV/c^2.

To reject the soft pions from D^{*+} decays, the momentum of any pion, which does not originate from a K_S^0, η, or η' decay, is required to be greater than 0.1 GeV/c. For the tag mode $D_s^- \to \pi^+\pi^-\pi^-$, the peaking background from $D_s^- \to K_S^0\pi^-$ final state is rejected by requiring any $\pi^+\pi^-$ combination to be outside of the mass window ± 0.03 GeV/c^2 around the K_S^0 nominal mass [20].

To suppress non-$D_s^\pm D_s^{*\mp}$ events, the beam-constrained mass of the single-tag D_s^- candidate,

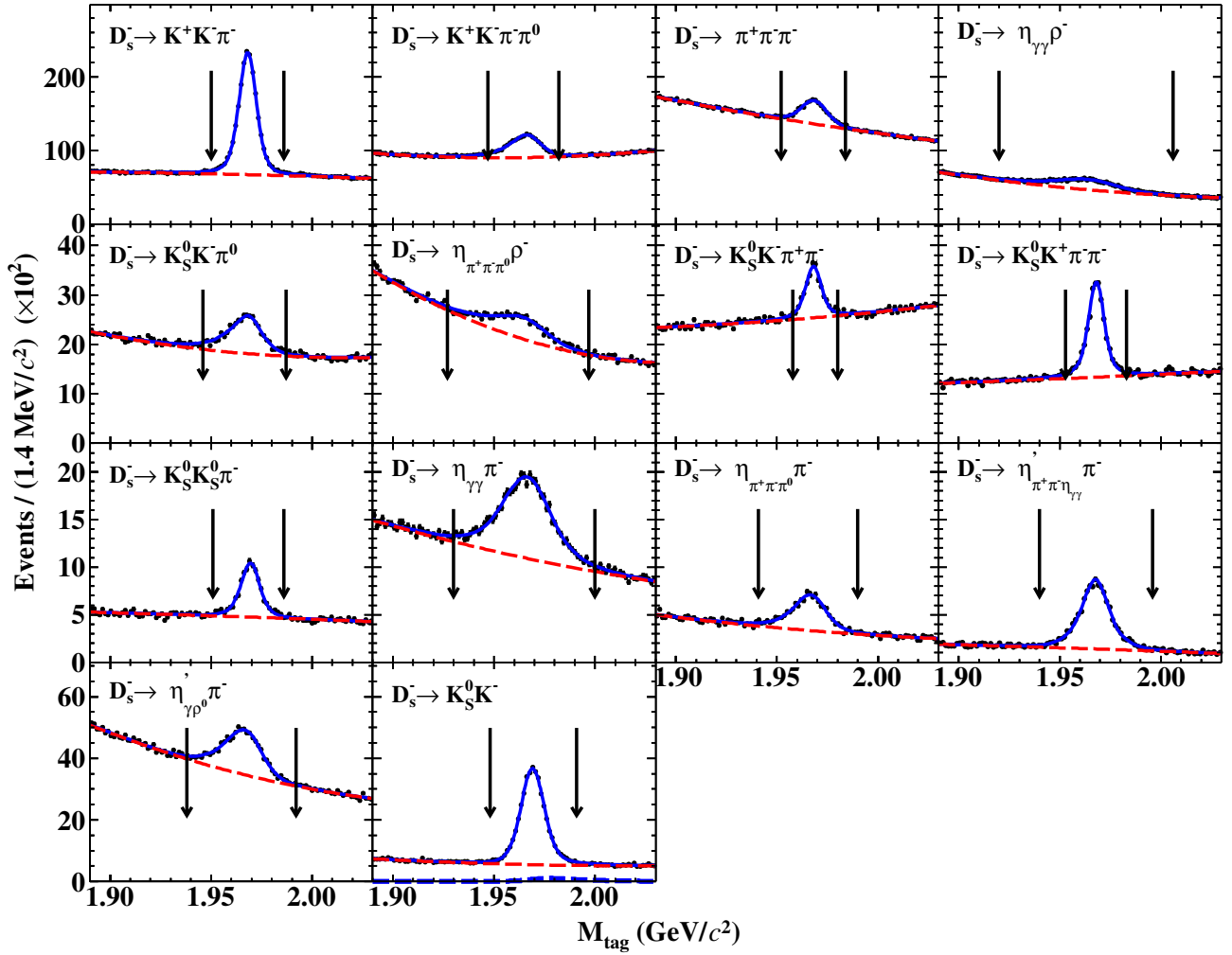$$M_{\text{BC}} \equiv \sqrt{E_{\text{beam}}^2 - |\vec{p}_{\text{tag}}|^2}, \tag{4}$$

FIG. 1.   Fits to the M_{tag} distributions of the accepted single-tag candidates from the data sample at $\sqrt{s} = 4.178$ GeV. Points with error bars are data. Blue solid curves are the fit results. Red dashed curves are the fitted backgrounds. Blue dotted curve in the $K_S^0 K^-$ mode is the $D^- \to K_S^0 \pi^-$ component. In each subfigure, the pair of arrows denote the signal regions.

is required to be within $(2.010, 2.070 + j \times 0.003)$ GeV/c^2, where E_{beam} is the beam energy, and $\vec{p}_{tag}$ is the momentum of the single-tag D_s^- candidate in the rest frame of the initial $e^+ e^-$ beams. This requirement retains most of the D_s^- mesons from $e^+ e^- \to D_s^{\pm} D_s^{*\mp}$.

In each event, we only keep one candidate with the D_s^- recoil mass,

$$M_{rec} \equiv \sqrt{\left(\sqrt{s} - \sqrt{|\vec{p}_{tag}|^2 + m_{D_s^-}^2}\right)^2 - |\vec{p}_{tag}|^2}, \quad (5)$$

closest to the D_s^{*+} nominal mass [20] per tag mode per charge. Figure 1 shows the invariant mass (M_{tag}) spectra of the accepted single-tag candidates for various tag modes. For each tag mode, the single-tag yield is obtained by a fit to the corresponding M_{tag} spectrum. The signal is described by the simulated shape convolved with a Gaussian function representing the difference in resolution between data and

simulation. For the tag mode $D_s^- \to K_S^0 K^-$, the peaking background from $D^- \to K_S^0 \pi^-$ is described by the simulated shape convolved with the same Gaussian function used in the signal shape, and its size is left as a free parameter. The nonpeaking background is modeled by a first- or second-order Chebychev polynomial function, which has been validated by using the inclusive simulation sample. The resultant fit results for the data sample taken at $\sqrt{s} = 4.178$ GeV are shown in Fig. 1. The candidates in the signal regions, denoted as the black arrows in each subfigure, are kept for further analysis. The backgrounds from $e^+ e^- \to (\gamma_{ISR}) D_s^+ D_s^-$, which contribute about (0.7–1.1)% in the fitted single-tag yields for various tag modes based on simulation, are subtracted in this analysis. As an example, the resulting single-tag yields (N_{ST}^{i1}) for various tag modes in data at $\sqrt{s} = 4.178$ GeV, and the corresponding single-tag efficiencies (ϵ_{ST}^{i1}) are summarized in the second and third columns of Table I, respectively. The

TABLE I.   The obtained values of N_{ST}^{i1}, $\epsilon_{\mathrm{ST}}^{i1}$, and $\epsilon_{\mathrm{DT}}^{i1}$ in the i-th tag mode at $\sqrt{s}$ = 4.178 GeV, where the efficiencies do not include the branching fractions for the subresonant decays, and the uncertainties are statistical only. The differences among the ratios of $\epsilon_{\mathrm{DT}}^{i1}$ over $\epsilon_{\mathrm{ST}}^{i1}$ for various modes are mainly due to the requirement of $E_{\mathrm{extra}\,\gamma}^{\mathrm{sum}}$.

Tag mode	N_{ST}^{i1} $(\times 10^3)$	$\epsilon_{\mathrm{ST}}^{i1}$ (%)	$\epsilon_{\mathrm{DT}}^{i1}$(%)
$K^+K^-\pi^-$	137.3 ± 0.6	40.90 ± 0.04	6.80 ± 0.04
$K^+K^-\pi^-\pi^0$	42.7 ± 0.9	11.81 ± 0.04	1.75 ± 0.02
$\pi^+\pi^-\pi^-$	36.4 ± 0.9	52.12 ± 0.21	11.87 ± 0.11
$K_S^0 K^-$	32.4 ± 0.3	49.73 ± 0.09	10.69 ± 0.11
$K_S^0 K^-\pi^0$	11.4 ± 0.3	17.07 ± 0.13	3.60 ± 0.07
$K_S^0 K_S^0\pi^-$	5.1 ± 0.1	22.77 ± 0.14	4.55 ± 0.12
$K_S^0 K^+\pi^-\pi^-$	14.8 ± 0.2	21.05 ± 0.07	3.54 ± 0.06
$K_S^0 K^-\pi^+\pi^-$	7.6 ± 0.3	18.47 ± 0.14	3.27 ± 0.08
$\eta_{\gamma\gamma}\pi^-$	19.4 ± 0.9	48.96 ± 0.21	10.57 ± 0.14
$\eta_{\pi^+\pi^-\pi^0}\pi^-$	5.7 ± 0.2	24.29 ± 0.16	5.61 ± 0.13
$\eta'_{\pi^+\pi^-\eta_{\gamma\gamma}}\pi^-$	9.8 ± 0.1	25.43 ± 0.09	5.35 ± 0.10
$\eta'_{\gamma\rho^0}\pi^-$	24.6 ± 0.7	32.51 ± 0.17	7.12 ± 0.09
$\eta_{\gamma\gamma}\rho^-$	40.8 ± 1.8	20.00 ± 0.11	4.33 ± 0.04
$\eta_{\pi^+\pi^-\pi^0}\rho^-$	11.0 ± 0.9	9.48 ± 0.11	2.07 ± 0.04

individual numbers of N_{ST}^{ij} and $\epsilon_{\mathrm{ST}}^{ij}$ at the other energy points are obtained similarly. The total single-tag yields N_{ST}^{j} at various energy points are summarized in the second column of Table II.

V. SELECTION OF $D_s^+ \to \tau^+\nu_\tau$

From the recoil of the single-tag D_s^- mesons, the candidates for $D_s^+ \to \tau^+\nu_\tau$ are selected via the $\tau^+ \to \pi^+\pi^0\bar{\nu}_\tau$ decay channel with the residual neutral showers and charged tracks. The transition $\gamma(\pi^0)$ from the D_s^{*+} and the leptonic D_s^+ decay signals are distinguished from combinatorial backgrounds by three kinematic variables,

$$\Delta E \equiv \sqrt{s} - E_{\mathrm{tag}} - E_{\mathrm{miss}} - E_{\gamma(\pi^0)},$$

and

TABLE II.   The total single-tag yields (N_{ST}^{j}) and the averaged signal efficiencies ($\epsilon_{\gamma(\pi^0)\tau^+\nu_\tau}^{j}$) at various energy points, where the efficiencies do not include the branching fractions for the subresonant decays, and the uncertainties are statistical only.

$\sqrt{s}$ (GeV)	N_{ST}^{j} $(\times 10^3)$	$\epsilon_{\gamma(\pi^0)\tau^+\nu_\tau}^{j}$(%)
4.178	398.8 ± 2.8	19.01 ± 0.06
4.189	61.4 ± 0.8	18.55 ± 0.14
4.199	61.4 ± 1.0	18.43 ± 0.15
4.209	57.5 ± 1.0	17.77 ± 0.14
4.219	47.9 ± 1.1	17.24 ± 0.15
4.226	80.8 ± 1.6	17.19 ± 0.14

$$\mathrm{MM}^{(*)2} \equiv (\sqrt{s} - \Sigma_k E_k)^2 - |-\Sigma_k \vec{p}_k|^2.$$

Here, $E_{\mathrm{miss}} \equiv \sqrt{|\vec{p}_{\mathrm{miss}}|^2 + m_{D_s^+}^2}$ and $\vec{p}_{\mathrm{miss}} \equiv -\vec{p}_{\mathrm{tag}} - \vec{p}_{\gamma(\pi^0)}$ are the missing energy and momentum of the recoiling system of the transition $\gamma(\pi^0)$ and the single-tag D_s^-, where E_k and $\vec{p}_k$ are the energy and momentum of the given particle k [$\pi^+\pi^0$, transition $\gamma(\pi^0)$ or tag], respectively. The MM^{*2} and MM^2 are the missing masses squared of the signal D_s^+ and neutrinos, respectively. The index k sums over the single-tag D_s^- and the transition $\gamma(\pi^0)$ for MM^{*2}, while over the single-tag D_s^-, the transition $\gamma(\pi^0)$ and $\pi^+\pi^0$ for MM^2. Here, the MM^{*2} is required to be within the interval $(3.82, 3.98)$ GeV$^2/c^4$. All remaining γ and π^0 candidates are looped over, and the one giving the least $|\Delta E|$ is chosen as the transition $\gamma(\pi^0)$ candidate. The $\tau^+ \to \pi^+\pi^0\bar{\nu}_\tau$ is actually dominated by $\tau^+ \to \rho^+\bar{\nu}_\tau$. To form the ρ^+ candidate of the signal side, we use the same selection criteria as those of the tag side. The charge of the pion candidate is required to be opposite to that of the single-tag D_s^- meson. To suppress the backgrounds with extra photon(s), the sum of the energies deposited in the EMC of those unused showers in the double-tag event ($E_{\mathrm{extra}\,\gamma}^{\mathrm{sum}}$) is required to be less than 0.1 GeV based on an optimization using the inclusive MC sample. Figure 2(a) shows the distribution of $E_{\mathrm{extra}\,\gamma}^{\mathrm{sum}}$ of the double-tag candidates. The consistency between data and MC simulation around zero is not very good. The associated acceptance efficiency difference due to imperfect simulation will be corrected as discussed later. Moreover, we require no extra good charged track in each event ($N_{\mathrm{extra}}^{\mathrm{charge}} = 0$).

To check the quality of the reconstructed ρ^+, we examine the $M_{\pi^+\pi^0}$ spectrum and the helicity angle of ρ^+ candidates ($\cos\theta_\rho$) of the selected double-tag candidates, as shown in Figs. 2(b) and 2(c). The θ_ρ is calculated as an angle of the momentum of π^+ in the rest frame of ρ^+, with respect to the ρ^+ direction in the initial e^+e^- beams, as the τ^+ momentum is not available. Figure 3 shows the resulting MM^2 distributions of the $D_s^+ \to \tau^+\nu_\tau$ candidates selected from the data samples at various energy points.

VI. BRANCHING FRACTION

The efficiencies of reconstructing the double-tag candidate events are determined with exclusive signal MC samples of $e^+e^- \to D_s^+D_s^{*-} + $ c.c., where the D_s^- decays to each tag mode, and the D_s^+ decays to $\tau^+\nu_\tau$ with $\tau^+ \to \pi^+\pi^0\bar{\nu}_\tau$. The double-tag efficiencies ($\epsilon_{\mathrm{DT}}^{i1}$) obtained at $\sqrt{s}$ = 4.178 GeV are summarized in the fourth column of Table I. The obtained $\epsilon_{\gamma(\pi^0)\tau^+\nu_\tau}^{j}$ at various energy points are summarized in the third column of Table II. These efficiencies have been corrected by a factor $f^{\mathrm{cor}} = 1.058 \times 0.996 \times 0.991 \times 1.003$ to take into account the data-MC efficiency differences due to the requirements of
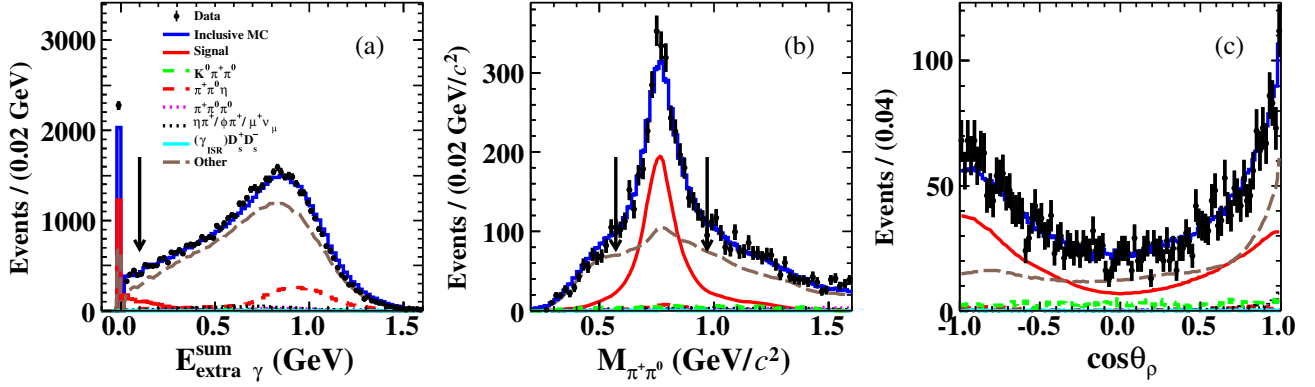
FIG. 2.   Distributions of (a) $E_{\text{extra}\,\gamma}^{\text{sum}}$, (b) $M_{\pi^+\pi^0}$, and (c) $\cos\theta_\rho$ of the selected $D^+ \to \tau^+\nu_\tau$ candidates summed over all tag modes from all data samples. Points with error bars are data. Blue solid lines are obtained from inclusive MC sample. Red solid lines show the signals. Green dashed, red dashed, pink dotted, black dotted, cyan solid, and brown dashed lines are the backgrounds from $D_s^+ \to K^0\pi^+\pi^0$, $D_s^+ \to \pi^+\pi^0\eta$, $D_s^+ \to \pi^+\pi^0\pi^0$, $D_s^+ \to (\eta\pi^+, \phi\pi^+, \mu^+\nu_\mu)$, $e^+e^- \to (\gamma_{\text{ISR}})D_s^+D_s^-$, and the other backgrounds after excluding the components aforementioned, respectively. In (a) and (b), the arrows show the corresponding requirements, and the events are imposed with all requirements except for the one to be shown.

$E_{\text{extra}\,\gamma}^{\text{sum}}$ & $N_{\text{extra}}^{\text{charge}}$, π^+ PID, MM^{*2}, and the least $|\Delta E|$ as described in Sec. VII.

To obtain the branching fraction for $D_s^+ \to \tau^+\nu_\tau$, we perform a simultaneous fit to the MM^2 distributions, as shown in Fig. 3, where the six energy points are constrained to have a common leptonic decay branching fraction. For various energy points, the branching fractions are calculated

by using Eq. (3) with N_{DT}^j, N_{ST}^j, and $\epsilon_{\gamma(\pi^0)\tau^+\nu_\tau}^j$. The shapes of the $D_s^+ \to \tau^+\nu_\tau$ signals are described by a sum of two bifurcated-Gaussian functions, whose parameters are determined from the fits to the signal MC events and are fixed in the simultaneous fit. The peaking backgrounds of $D_s^+ \to K^0\pi^+\pi^0$ [42], $D_s^+ \to \pi^+\pi^0\pi^0$ [20], $D_s^+ \to \pi^+\pi^0\eta$ [43], $D_s^+ \to \eta\pi^+$ [20], $D_s^+ \to \phi\pi^+$ [20], and $D_s^+ \to \mu^+\nu_\mu$ [8]

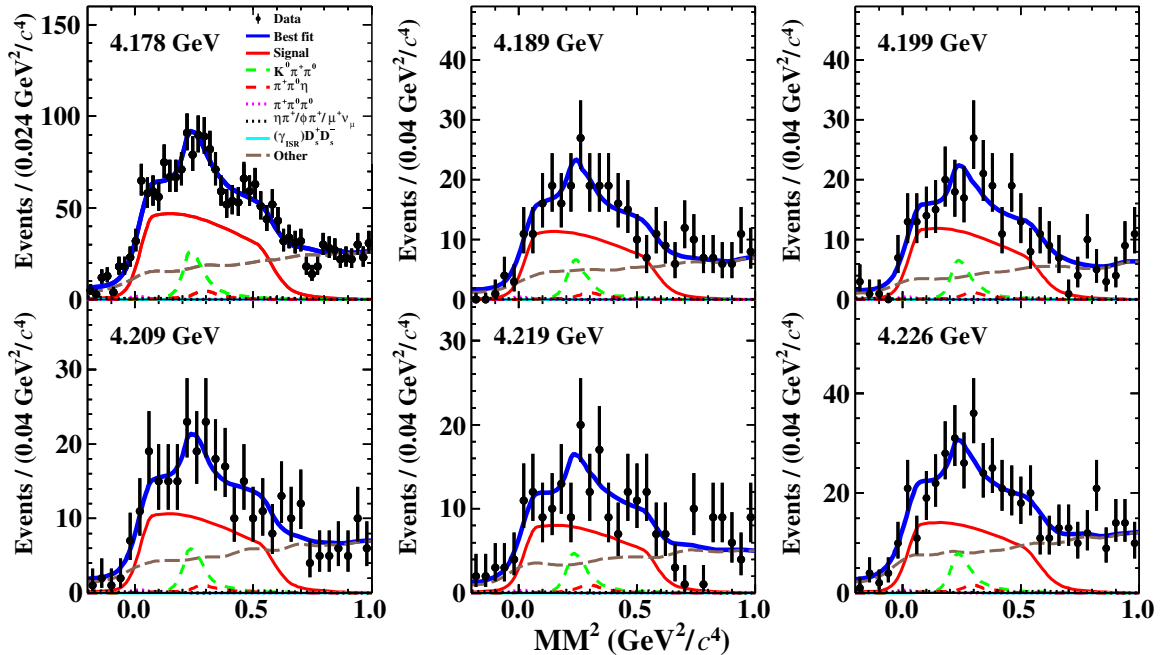
FIG. 3.   Simultaneous fit to the MM^2 distributions of the accepted $D_s^+ \to \tau^+\nu_\tau$ candidates from the data samples at various energy points. Points with error bars are data. Solid blue curves are the fit results. Red solid lines show the signals. Green dashed, red dashed, pink dotted, black dotted, cyan solid, and brown dashed curves are the backgrounds from $D_s^+ \to K^0\pi^+\pi^0$, $D_s^+ \to \pi^+\pi^0\eta$, $D_s^+ \to \pi^+\pi^0\pi^0$, $D_s^+ \to (\eta\pi^+, \phi\pi^+, \mu^+\nu_\mu)$, $e^+e^- \to (\gamma_{\text{ISR}})D_s^+D_s^-$, and the other backgrounds after excluding the components aforementioned, respectively.

are modeled by the corresponding simulated shapes. The $D_s^+ \to \pi^+\pi^0\eta$ decays are generated using the amplitude-analysis results in Ref. [43]. The $D_s^+ \to \eta\pi^+$, $D_s^+ \to \phi\pi^+$, and $D_s^+ \to \mu^+\nu_\mu$ decays are uniformly generated across the event phase space. To model the resonant contributions in the $D_s^+ \to K^0\pi^+\pi^0$ and $D_s^+ \to \pi^+\pi^0\pi^0$ decays, these two decays are generated with a modified data-driven generator BODY3 [35,44], which was developed to simulate different intermediate states in data for a given three-body final state. The two-dimensional distributions of $M_{K^0\pi^+}^2$ versus $M_{\pi^+\pi^0}^2$ and $M_{\pi^+\pi^0}^2$ versus $M_{\pi^0\pi^0}^2$ found in data, corrected for backgrounds and efficiencies, are taken as the input for the BODY3 generator. The efficiencies across the kinematic space are obtained with the MC samples generated with the modified phase-space generator. For $D_s^+ \to K^0\pi^+\pi^0$, the interaction between the K_L^0 particle and the EMC materials may not be well simulated, thus causing a large difference between the acceptance efficiency of data and that of simulation due to the requirement of $E_{\text{extra}\,\gamma}^{\text{sum}} < 0.1$ GeV. Therefore, the sizes of the $D_s^+ \to K^0\pi^+\pi^0$ background are float, but their rates over the simulated ones at the six energy points are constrained to be the same. The yields of the peaking backgrounds of $D_s^+ \to \pi^+\pi^0\pi^0$, $D_s^+ \to \pi^+\pi^0\eta$, $D_s^+ \to \eta\pi^+$, $D_s^+ \to \phi\pi^+$, and $D_s^+ \to \mu^+\nu_\mu$ are estimated based on the MC simulated misidentification efficiencies and the world average branching fractions, and their sizes are fixed in the fit. The simulated shapes of these peaking backgrounds have been smeared with a Gaussian function, with parameters obtained from the control sample of $D_s^+ \to \eta\rho^+$. The background of $D_s^- \to$ tags versus $D_s^+ \to$ signals from $e^+e^- \to (\gamma_{\text{ISR}})D_s^+D_s^-$ contributes about 0.3% of the observed signal yield, and its relative ratio is also fixed in the fit. The other combinatorial backgrounds are modeled by the shapes from the inclusive MC sample after excluding the components aforementioned.

The simultaneous fit results are also shown in Fig. 3. From this fit, the branching fraction for $D_s^+ \to \tau^+\nu_\tau$ is obtained to be $(5.29 \pm 0.25)\%$. This corresponds to the signal yield of $D_s^+ \to \tau^+\nu_\tau$ to be 1745 ± 84, where the uncertainty is statistical only.

VII. SYSTEMATIC UNCERTAINTIES

With the DT method, most of uncertainties related to the single-tag selection are canceled. Sources of the systematic uncertainties in the branching fraction measurement are summarized in Table III. Each of them, which is estimated relative to the measured branching fraction, is described below.

A. Determination of single-tag yield

The uncertainty in the total number of the single-tag D_s^- mesons is assigned to be 0.6% by taking into account the

TABLE III. Systematic uncertainties in the branching fraction measurement.

Source	Uncertainty (%)
Single-tag yield	0.6
π^+ tracking	0.2
π^+ PID	0.2
$\gamma(\pi^0)$ reconstruction	2.1
$E_{\text{extra}\,\gamma}^{\text{sum}}$ and $N_{\text{extra}}^{\text{charge}}$ requirements	2.2
MM^{*2} requirement	0.8
τ^+ decay	1.2
MM^2 fit	1.3
Least $|\Delta E|$	0.4
Tag bias	0.5
MC statistics	0.3
Quoted branching fractions	0.5
Total	3.8

background fluctuation in the fit and examining the changes of the fit yields when varying the signal shape and background shape.

B. π^+ tracking and PID

The π^+ tracking and PID efficiencies are studied with the $e^+e^- \to K^+K^-\pi^+\pi^-$ events. The data-MC efficiency ratios of the π^+ tracking and PID efficiencies are 1.000 ± 0.002 and 0.996 ± 0.002, respectively. After multiplying the signal efficiencies by the latter factor, we assign 0.2% and 0.2% as the systematic uncertainties arising from the π^+ tracking and PID efficiencies, respectively.

C. $\gamma(\pi^0)$ reconstruction

The photon selection efficiency was previously studied with the $J/\psi \to \pi^+\pi^-\pi^0$ decays [45]. The π^0 reconstruction efficiency was previously studied with the $e^+e^- \to K^+K^-\pi^+\pi^-\pi^0$ events. The systematic uncertainty of finding the transition $\gamma(\pi^0)$, which is weighted according to the branching fractions for $D_s^{*+} \to \gamma D_s^+$ and $D_s^{*+} \to \pi^0 D_s^+$ [20], is obtained to be 1.0%. For the π^0 in the leptonic decay, the relevant systematic uncertainty is assigned to be 1.1%. The total systematic uncertainty related to the photon and π^0 reconstruction is obtained to be 2.1% by adding these two uncertainties linearly.

D. $E_{\text{extra}\,\gamma}^{\text{sum}}$ and $N_{\text{extra}}^{\text{charge}}$ requirements

The efficiencies for the combined requirements of $E_{\text{extra}\,\gamma}^{\text{sum}}$ and $N_{\text{extra}}^{\text{charge}}$ are investigated with the double-tag sample of $D_s^+ \to \eta\pi^+$, which has similar acceptance efficiencies to our signals. The ratio of the averaged efficiency of data to that of simulation is 1.058 ± 0.022. After multiplying the signal efficiency by this factor, we assign 2.2% as the relevant systematic uncertainty.

E. MM^{*2} requirement

To assign the systematic uncertainty originating from the MM^{*2} requirement, we fit to the MM^{*2} distribution of the accepted $D^+ \to \tau^+ \nu_\tau$ candidates in data after excluding this requirement. In the fit, the background shape is derived from the inclusive MC sample, and the signal shape is described by the shape from the signal MC events convolved with a Gaussian function to take into account the difference between data and simulation. The parameters of the Gaussian function are floated. From the fit, the mean and resolution of the Gaussian function are obtained to be 0.008 GeV$^2/c^4$ and 0.012 GeV$^2/c^4$, respectively. Then, we examine the signal efficiency after smearing the corresponding Gaussian function to the MM^{*2} variable. The ratio of the acceptance efficiencies with and without the smearing is 0.991 ± 0.008. After multiplying the signal efficiency by the factor, we assign 0.8% as the systematic uncertainty of the MM^{*2} requirement.

F. τ^+ decay

The difference of the measured branching fractions with and without taking into account $\tau^+ \to (\pi^+ \pi^0)_{\text{non}-\rho} \bar{\nu}_\tau$ [20], 1.2%, is considered as a systematic uncertainty. The uncertainty due to imperfect simulation of the $M_{\pi^+ \pi^0}$ line shape is assigned with the same method described in Sec. VII E. From the fit to the $M_{\pi^+ \pi^0}$ distribution of data, the mean and resolution of the Gaussian function used to smear the $M_{\pi^+ \pi^0}$ distribution are obtained to be $(0.010, 0.008)$ GeV/c^2. The difference of the signal efficiencies with and without smearing is negligible.

G. MM^2 fit

The systematic uncertainty in the MM^2 fit is considered in three aspects. At first, we vary the estimated yields of peaking backgrounds from $D_s^+ \to K^0 \pi^+ \pi^0$ [42], $D_s^+ \to \pi^+ \pi^0 \pi^0$ [20], $D_s^+ \to \pi^+ \pi^0 \eta$ [43], $D_s^+ \to \eta \pi^+$ [20], $D_s^+ \to \phi \pi^+$ [20], and $D_s^+ \to \mu^+ \nu_\mu$ [8] by $\pm 1\sigma$ of the quoted branching fractions and the input cross section [46]. Then, we vary the peaking background yields of $D_s^+ \to \pi^+ \pi^0 \eta$ and $D_s^+ \to \pi^+ \pi^0 \pi^0$ by -20%, based on the data-MC difference of the inefficiency of photon(s). Finally, we float the parameters of two bifurcated-Gaussian functions and the convoluted Gaussian functions by $\pm 1\sigma$. The quadratic sum of the relative changes of the remeasured branching fractions, 1.3%, is assigned as the corresponding systematic uncertainty.

H. Selection of the transition $\gamma(\pi^0)$ with the least $|\Delta E|$

The systematic uncertainty from the selection of the transition $\gamma(\pi^0)$ from D_s^{*+} with the least $|\Delta E|$ method is estimated by using the control samples of $D_s^+ \to K^+ K^- \pi^+$ and $D_s^+ \to \eta \pi^0 \pi^+$. The ratio of the efficiency of selecting

the transition $\gamma(\pi^0)$ candidates of data to that in simulation is 1.003 ± 0.004. After multiplying the signal efficiency by this factor, we take 0.4% as the corresponding systematic uncertainty.

I. Tag bias

The single-tag efficiencies in the inclusive and signal MC samples may be slightly different from each other due to different track multiplicities in these two environments. This may cause incomplete cancellation of the uncertainties of the single-tag selection efficiencies. The associated uncertainty is assigned as 0.5% by taking into account the differences of the tracking and PID efficiencies of $K^\pm$ and $\pi^\pm$, as well as the selections of neutral particles between data and simulation in different environments.

J. MC statistics

The uncertainty due to the finite MC statistics 0.3%, which is dominated by that of the double-tag efficiency, is considered as a source of systematic uncertainty.

K. Quoted branching fractions

The uncertainties of the quoted branching fractions for $\pi^0 \to \gamma\gamma$ and $\tau^+ \to \pi^+ \pi^0 \bar{\nu}_\tau$ are 0.03% and 0.4%, respectively. The world average branching fractions for $D_s^{*-} \to \gamma D_s^-$ and $D_s^{*-} \to \pi^0 D_s^-$ are $(93.5 \pm 0.7)\%$ and $(5.8 \pm 0.7)\%$, respectively, which are fully correlated with each other. An associated uncertainty is assigned by reweighting $\varepsilon_{\gamma\tau^+\nu_\tau}$ and $\varepsilon_{\pi^0\tau^+\nu_\tau}$ via varying these two branching fractions by $\pm 1\sigma$. The change of the reweighted signal efficiency is 0.2%. The uncertainty of the branching fraction for $D_s^{*-} \to e^+ e^- D_s^-$, 0.2%, is considered as an additional uncertainty. The total systematic uncertainty associated with the above branching fractions is obtained to be 0.5%, by adding these four uncertainties in quadrature.

L. Total systematic uncertainty

The total systematic uncertainty in the measurement of the branching fraction for $D_s^+ \to \tau^+ \nu_\tau$ is determined to be 3.8% by adding all above uncertainties in quadrature.

VIII. RESULTS

Combining our branching fraction,

$$\mathcal{B}_{D_s^+ \to \tau^+ \nu_\tau} = (5.29 \pm 0.25_{\text{stat}} \pm 0.20_{\text{syst}})\%,$$

and the world average values of G_F, m_μ, $m_{D_s^+}$, and $\tau_{D_s^+}$ [20] in Eq. (1) with $\Gamma_{D_s^+ \to \tau^+ \nu_\tau} = \mathcal{B}_{D_s^+ \to \tau^+ \nu_\tau}/\tau_{D_s^+}$ yields

$$f_{D_s^+}|V_{cs}| = (244.8 \pm 5.8_{\text{stat}} \pm 4.8_{\text{syst}}) \text{ MeV}.$$

Here, the systematic uncertainties arise mainly from the uncertainties in the measured branching fraction (3.8%)

and the D_s^+ lifetime (0.8%). Taking $|V_{cs}| = 0.97320 \pm 0.00011$ from the global fit in the standard model [20,47], we obtain $f_{D_s^+} = (251.6 \pm 5.9_{\text{stat}} \pm 4.9_{\text{syst}})$ MeV. Alternatively, taking $f_{D_s^+} = (249.9 \pm 0.5)$ MeV of the recent LQCD calculations [10–13] as input, we determine $|V_{cs}| = 0.980 \pm 0.023_{\text{stat}} \pm 0.019_{\text{syst}}$. One additional systematic uncertainty of the input $f_{D_s^+}$ is 0.2%, while that of $|V_{cs}|$ is negligible. The $|V_{cs}|$ measured in this work is in agreement with our measurements via the $D \to \bar{K}\ell^+\nu_\ell$ decays [48–51], the $D_s^+ \to \mu^+\nu_\mu$ decay [8], and the $D_s^+ \to \eta^{(\prime)}e^+\nu_e$ decays [40].

Using the branching fraction of $\mathcal{B}_{D_s^+ \to \mu^+\nu_\mu} = (5.35 \pm 0.21) \times 10^{-3}$ [9], $\mathcal{R}_{\tau/\mu}$ is determined to be 9.89 ± 0.71, which agrees with the standard model predicted value of 9.75 ± 0.01 within 1σ.

IX. SUMMARY

By analyzing 6.32 fb^{-1} of e^+e^- collision data collected between 4.178 and 4.226 GeV with the BESIII detector, we present a measurement of $D_s^+ \to \tau^+\nu_\tau$ using the $\tau^+ \to \pi^+\pi^0\bar{\nu}_\tau$ decay channel. The branching fraction for $D_s^+ \to \tau^+\nu_\tau$ is determined to be $(5.29 \pm 0.25 \pm 0.20)\%$, which is well consistent with previous measurements [20]. Combining this branching fraction with the $|V_{cs}|$ given by CKMfitter [20,47], we obtain $f_{D_s^+} = (251.6 \pm 5.9 \pm 4.9)$ MeV. Conversely, combining this branching fraction with the $f_{D_s^+}$ calculated by the latest LQCD [10–13], we determine $|V_{cs}| = 0.980 \pm 0.023 \pm 0.019$. Combining our branching fraction with $\mathcal{B}(D_s^+ \to \mu^+\nu_\mu) = (5.35 \pm 0.21) \times 10^{-3}$ [9], we determine $\mathcal{R}_{\tau/\mu} = 9.89 \pm 0.71$, which is consistent with the expectation based on lepton flavor universality. This ratio implies that no lepton flavor universality violation is found between the $D_s^+ \to \tau^+\nu_\tau$ and $D_s^+ \to \mu^+\nu_\mu$ decays under the current precision. Combining our branching fraction with the one measured via $\tau^+ \to \pi^+\bar{\nu}_\tau$ [9], we obtain $\mathcal{B}(D_s^+ \to \tau^+\nu_\tau) = (5.24 \pm 0.18 \pm 0.14)\%$, $f_{D_s^+} = (250.4 \pm 4.3 \pm 3.4)$ MeV, $|V_{cs}| = 0.975 \pm 0.017 \pm 0.013$, and $\mathcal{R}_{\tau/\mu} = 9.79 \pm 0.57$, where the uncertainties from the single-tag yield, the $\pi^\pm$ tracking efficiency, the soft γ reconstruction, the best transition photon selection, and

[1] D. Silverman and H. Yao, Phys. Rev. D **38,** 214 (1988).

[2] J. P. Alexander *et al.* (CLEO Collaboration), Phys. Rev. D **79,** 052001 (2009).

[3] P. Naik *et al.* (CLEO Collaboration), Phys. Rev. D **80,** 112004 (2009).

[4] P. U. E. Onyisi *et al.* (CLEO Collaboration), Phys. Rev. D **79,** 052002 (2009).

[5] P. del Amo Sanchez *et al.* (*BABAR* Collaboration), Phys. Rev. D **82,** 091103 (2010).

[6] A. Zupanc *et al.* (Belle Collaboration), J. High Energy Phys. 09 (2013) 139.

[7] M. Ablikim *et al.* (BESIII Collaboration), Phys. Rev. D **94,** 072004 (2016).

[8] M. Ablikim *et al.* (BESIII Collaboration), Phys. Rev. Lett. **122,** 071802 (2019).

[9] M. Ablikim *et al.* (BESIII Collaboration), arXiv:2102.11734.

[10] A. Bazavov *et al.* (Fermilab Lattice and MILC Collaborations), Phys. Rev. D **98,** 074512 (2018).

[11] A. Bazavov *et al.* (Fermilab Lattice and MILC Collaborations), Phys. Rev. D **90,** 074509 (2014).

[12] N. Carrasco *et al.* (ETM Collaboration), Phys. Rev. D **91,** 054507 (2015).

[13] S. Aoki *et al.* (Flavour Lattice Averaging Group), Eur. Phys. J. C **80,** 113 (2020).

[14] P. A. Boyle, L. D. Debbio, A. Juttner, A. Khamseh, F. Sanfilippo, and J. T. Tsang, J. High Energy Phys. 12 (2017) 008.

[15] Y. Yi-Bo *et al.*, Phys. Rev. D **92,** 034517 (2015).

[16] W. P. Chen, Y. C. Chen, T. W. Chiu, H. Y. Chou, T. S. Guu, and T. H. Hsieh, Phys. Lett. B **736,** 231 (2014).

[17] D. Becirevic, B. Blossier, A. Gerardin, A. L. Yaouanc, and F. Sanfilippo, Nucl. Phys. **B872,** 313 (2013).

[18] Z. G. Wang, Eur. Phys. J. C **75,** 427 (2015).

[19] H. B. Li and X. R. Lyu, arXiv:2103.00908.

[20] P. A. Zyla *et al.* (Particle Data Group), Prog. Theor. Exp. Phys. **2020,** 083C01 (2020).

[21] J. P. Lees *et al.* (*BABAR* Collaboration), Phys. Rev. Lett. **109,** 101802 (2012).

[22] J. P. Lees *et al.* (*BABAR* Collaboration), Phys. Rev. D **88,** 072012 (2013).

[23] R. Aaij *et al.* (LHCb Collaboration), Phys. Rev. Lett. **115,** 111803 (2015).

[24] M. Huschle *et al.* (Belle Collaboration), Phys. Rev. D **92,** 072014 (2015).

[25] Y. Sato *et al.* (Belle Collaboration), Phys. Rev. D **94,** 072007 (2016).

[26] R. Aaij *et al.* (LHCb Collaboration), Phys. Rev. D **97,** 072013 (2018).

[27] A. Abdesselam *et al.* (Belle Collaboration), arXiv:1904.08794.

[28] M. Ablikim *et al.* (BESIII Collaboration), Nucl. Instrum. Methods Phys. Res., Sect. A **614,** 345 (2010).

[29] C. H. Yu *et al.*, in *Proceedings of IPAC2016, Busan, Korea, 2016*, .

[30] M. Ablikim *et al.* (BESIII Collaboration), Chin. Phys. C **44,** 040001 (2020).

[31] X. Li *et al.*, Radiat. Detect. Technol. Methods **1,** 13 (2017); Y. X. Guo *et al.*, Radiat. Detect. Technol. Methods **1,** 15

(2017); P. Cao *et al.*, Nucl. Instrum. Methods Phys. Res., Sect. A **953,** 163053 (2020).

[32] S. Agostinelli *et al.* (GEANT4 Collaboration), Nucl. Instrum. Methods Phys. Res., Sect. A **506,** 250 (2003).

[33] S. Jadach, B. F. L. Ward, and Z. Was, Phys. Rev. D **63,** 113009 (2001); Comput. Phys. Commun. **130,** 260 (2000).

[34] R. G. Ping, Chin. Phys. C **38,** 083001 (2014).

[35] D. J. Lange, Nucl. Instrum. Methods Phys. Res., Sect. A **462,** 152 (2001); R. G. Ping, Chin. Phys. C **32,** 599 (2008).

[36] C. Patrignani *et al.* (Particle Data Group), Chin. Phys. C **40,** 100001 (2016).

[37] J. C. Chen, G. S. Huang, X. R. Qi, D. H. Zhang, and Y. S. Zhu, Phys. Rev. D **62,** 034003 (2000); R. L. Yang, R. G. Ping, and H. Chen, Chin. Phys. Lett. **31,** 061301 (2014).

[38] E. Richter-Was, Phys. Lett. B **303,** 163 (1993).

[39] R. M. Baltrusaitis *et al.* (MARK III Collaboration), Phys. Rev. Lett. **56,** 2140 (1986); J. Adler *et al.* (MARK III Collaboration), Phys. Rev. Lett. **60,** 89 (1988).

[40] M. Ablikim *et al.* (BESIII Collaboration), Phys. Rev. Lett. **122,** 121801 (2019).

[41] M. Ablikim *et al.* (BESIII Collaboration), Phys. Rev. D **99,** 072002 (2019).

[42] M. Ablikim *et al.* (BESIII Collaboration), arXiv:2103.15098v1.

[43] M. Ablikim *et al.* (BESIII Collaboration), Phys. Rev. Lett. **123,** 112001 (2019).

[44] M. Ablikim *et al.* (BESIII Collaboration) Phys. Rev. Lett. **124,** 241803 (2020).

[45] M. Ablikim *et al.* (BESIII Collaboration), Phys. Rev. D **83,** 112005 (2011).

[46] M. Ablikim *et al.* (BESIII Collaboration), Measuurement of the cross section for $e^+e^- \to D_s^\pm D_s^{*\mp}$ up to 4.7 GeV (to be published).

[47] J. Charles, A. Höcker, H. Lacker, S. Laplace, F. R. Le Diberder, J. Malclés, J. Ocariz, M. Pivk, and L. Roos (CKMfitter Group), Eur. Phys. J. C **41,** 1 (2005), updated results and plots available at http://ckmfitter.in2p3.fr.

[48] M. Ablikim *et al.* (BESIII Collaboration), Phys. Rev. D **92,** 072012 (2015).

[49] M. Ablikim *et al.* (BESIII Collaboration), Phys. Rev. D **96,** 012002 (2017).

[50] M. Ablikim *et al.* (BESIII Collaboration), Phys. Rev. D **92,** 112008 (2015).

[51] M. Ablikim *et al.* (BESIII Collaboration), Phys. Rev. Lett. **122,** 011804 (2019).